Original article

Crystallization and magnetic characterizations of DyIG and HoIG nanopowders fabricated using citrate sol-gel

CrossMark

Dao Thi Thuy Nguyet [a, *], Nguyen Phuc Duong [a, b], Takuya Satoh [c], Luong Ngoc Anh [a], To Thanh Loan [a], Than Duc Hien [a]

[a] International Training Institute for Materials Science (ITIMS), Hanoi University of Science and Technology, 1 Dai Co Viet Road, Hanoi, Viet Nam
[b] Vietnam-Japan International Institute for Science of Technology (VJIIST), Hanoi University of Science and Technology, 1 Dai Co Viet Road, Hanoi, Viet Nam
[c] Department of Physics, Kyushu University, 819-0395 Fukuoka, Japan

ARTICLE INFO

ABSTRACT

Dy and Ho iron garnets in form of nanoparticles were synthesized by citrate sol-gel method. Phase formation, lattice constant and average crystallite sizes of the samples were determined via XRD measurements. Morphology and particle size distribution were studied by TEM and chemical composition was checked by EDX. Magnetic measurements in temperature range 5—600 K and in the maximum applied field of 50 kOe were carried out by using SQUID and VSM. Their magnetic parameters, including Curie temperature, magnetization compensation temperature, spontaneous magnetization, high-field susceptibility, magnetic coercivity were discussed in the framework of three interacting magnetic sublattices, magnetocrystalline anisotropy, core-shell model and compared to those of the bulk materials. Based on these analyses further evaluation on the crystallinity and homogeneity of the samples has been made.

1. Introduction

Rare-earth iron garnet (RIG) of general formula $R_3Fe_5O_{12}$ (R is a rare earth element) crystallizes in cubic structure with the space group Ia3d. The magnetic ions are distributed over three crystallographic sites with sublattice magnetizations M_a (octahedral site 16a; [Fe^{3+}]), M_d (tetrahedral site 24d; (Fe^{3+})) and M_c (dodecahedral site 24c; {R^{3+}}). The two magnetic iron sublattices are antiparallel and their strong superexchange interactions decide the magnitude of the Curie temperature. The magnetic sublattice of the rare-earth ions is polarized by the iron sublattices and becomes magnetically oriented antiparallel to the resultant iron ion sublattice magnetization. In RIG, the exchange field between the Fe and rare-earth sublattices is much weaker than that between the two iron sublattices. The interaction between the R ions is very weak and the rare-earth sublattice can be considered to be essentially a system of paramagnetic ions situated in an exchange field created by the Fe sublattices. Due to the difference in the temperature dependence of the magnetization of sublattices, the net magnetization falls to zero at the so-called magnetization compensation temperature T_{comp}. For the non-S-state rare-earth ions, at low temperatures when both crystal field and exchange anisotropies become of the same order of magnitude, their magnetic moments will be canted relative to the usual easy direction [111] [1].

Miniaturization of new generation electronic devices requires the use of materials with nanometric dimensions. Recent studies on nanosized garnet compounds focus on the application in the field of microwave devices [2], high-density magnetic, magneto-optical information storage [3–5] and cryogenic magnetic refrigeration [6]. Although the magnetic properties of garnet bulks have been investigated through the past decades [see e.g. [7–10]], the complete understanding of their magnetic properties in nanoparticulate forms remains a challenge. These properties are known to be very sensitive to the physical characteristics such as the size, shape and surface properties of particles. Therefore, studying about manufacturing methods and the properties of rare-earth iron garnets in nano size is necessary and expands the applicability of the material. Up to now there are still few reports in the literature on the structural and magnetic properties of single phase nanocrystalline RIG garnets which were prepared by chemical sol-gel methods [11–14], glycine assisted combustion [15] or by mechanical milling [6,16,17]. It was found that in general the reduction in particle size causes the decrease in saturation magnetization. This

* Corresponding author. Tel.: +84 4 38680787; fax: +84 4 38692963.
E-mail address: nguyet@itims.edu.vn (D.T.T. Nguyet).
Peer review under responsibility of Vietnam National University, Hanoi.

decrease of the saturation magnetization may be attributed to the existence of a non-magnetic surface layer [18] or to a non-collinear spin arrangement at the surface of the particles [19]. In ferrous oxide nanoparticles, oxygen vacancies may exist which result in a change of the oxidation state of iron ions for charge compensation. Guillot et al. via magnetization and Mössbauer measurements have proved that the synthesis of nanocrystalline GdIG and DyIG by ball milling leads to a partial reduction of Fe^{3+} (S = 5/2) to Fe^{2+} (S = 2) and hence the cation distribution was changed compared to the source bulks [16,17].

In our recent studies, single-phase yttrium and gadolinium iron garnets were successfully prepared by using citrate sol-gel followed by heat-treatment at 800 °C [13,14]. This method allows a good mixing of the chemical components in the reaction at atomic scales based on that homogenous samples can be achieved. In addition, by using this method single-phase nanoparticles can be obtained at annealing temperatures lower than those used in other fabrication methods. In these materials Y sublattice is non magnetic while Gd sublattice carries magnetic moment but has no anisotropy due to the S state of Gd ions.

In this work, preparation technology and magnetization characterization of rare-earth iron garnet nanoparticle systems with R = Dy and Ho were considered. Different from the case of gadolinium, in the cases of dysprosium and holmium due to the non-S state of the rare-earth ions both spin and orbital moments of the $4f$ electrons and the crystalline electric field influence the magnetic properties. The magnetic behaviors of the nanosized Dy and Ho iron garnets in external applied magnetic field are therefore expected to be different from those of the GdIG counterpart. The spontaneous magnetization, high-field susceptibility and coercivity of the samples were investigated in temperature range from 5 K to above the Curie temperature and discussed based on the size reduction effects.

2. Experiments

The sample fabrication route followed the steps described in our previous reports [13,14]. The gels were obtained from aqueous solutions of citric acid, nitrates of Fe^{3+} and R^{3+} (R = Dy, Ho) and then NH_4OH was added to adjust pH to ~10. The nanoparticle samples labeled as DyIGNPs and HoIGNPs were obtained after annealing the gel products at 800 °C in 2 h.

X-ray diffraction (Cu-Kα, Siemens D-5000) was employed to identify the phase formation, crystal structure and the average crystallite size on applying Rietveld method using FullProf program [20]. The diffraction peaks were modeled by pseudo−Voigt function. The refinement fitting quality was checked by goodness of fit (χ^2) and weighted profile R-factor (R_{wp}). The calculated results are accepted when χ^2 should approach 1 and R_{wp} must be close to or less than 10% [21].

Transmission electron microscope (JEOL 1010 − TEM) was used to examine the particle size and morphology. For TEM measurements, the particles were dispersed by rigorous vibration in ethanol for 4 h using ultrasonic. The concentrations of metal ions were determined using energy dispersive X-ray spectroscopy (EDX). For each sample, the elemental analysis was carried out at 4 different positions on the particle assembly. The magnetization loops in the temperature range from 5 K to room temperature were measured using a superconducting quantum interference device (SQUID) by Quantum Design with applied magnetic fields H up to 50 kOe and those at high temperatures were collected in vibrating sample magnetometer (VSM) with maximum field H = 10 kOe. For the magnetic measurements, the nanoparticles were fixed in nonmagnetic sample holder.

3. Results and discussion

3.1. Structure and morphology characterization

The XRD patterns of the samples and their Rietveld refinement are shown in Fig. 1. The refinement result indicates that all the samples are cubic and well refined in space group *Ia3d* with atoms in positions Fe1 in 16a(0, 0, 0), Fe2 in 24d(3/8, 0, 1/4), R in 24c(1/8, 0, 1/4) and O in 96h(x, y, z). None of impurity phases such as hematite (α-Fe_2O_3) or orthoferrite $RFeO_3$ is observed. The refined values of structural parameters including lattice constants (a), oxygen coordinate, parameters of microstructure (D, ε) and fitting quality are given in Table 1. The lattice constant of the samples are in good agreement with those reported for the bulks [7]. The smaller lattice constant of HoIGNPs compared to DyIGNPs can be explained due to the smaller ionic radii of Ho^{3+} compared to that of Dy^{3+} (r_{Ho}^{3+} = 1.155 Å; r_{Dy}^{3+} = 1.167 Å for dodecahedral site).

The mass density of these samples was determined via the relation

$$\rho_{XRD} = 8M \Big/ \left(N_A a^3 \right) \qquad (1)$$

where M is the mole mass in gram, 8 number of chemical formula units per unite cell, a the lattice constant and N_A the Avogadro constant. ρ_{XRD} is found to be 6.7 g/cm^3 and 6.75 g/cm^3 for DyIGNPs and HoIGNPs, respectively.

The microstructure parameters including average size of coherent scattering region D (usually called the crystallite size) and lattice microstrains $\Delta a/a$ (where a is lattice constant) were obtained by analysis of the peak broadening (Table 1). In our work the average size of coherent scattering region and the microstrains were determined on applying Rietveld method using FullProf program with condition that instrumental resolution function was
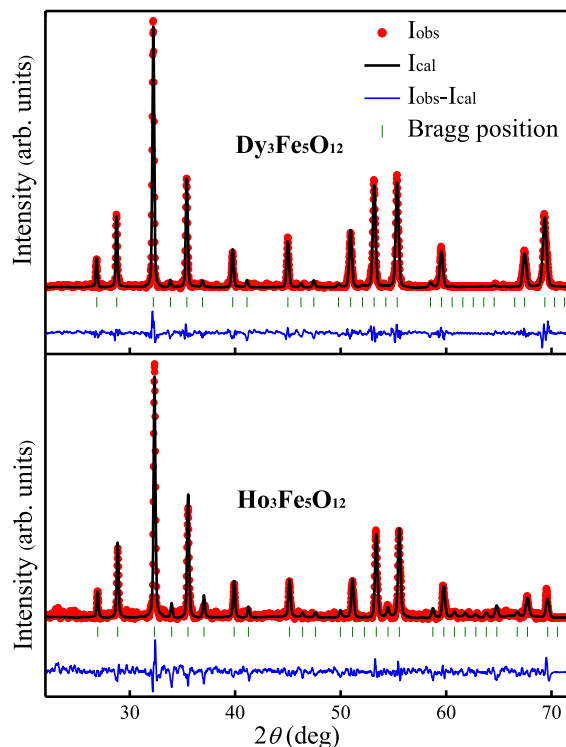

Fig. 1. X-ray diffraction patterns of samples and processed by the Rietveld method. The experimental points as well as calculated and difference functions are indicated.

Table 1
Structural parameters of the samples estimated from Rietveld refinement: lattice constant (a), oxygen coordinate, crystallite size (D), microstrain ($\Delta a/a$) and fitting quality (χ^2 and R_{wp}).

Sample	a, Å	Oxygen coordinate			D, nm	$\Delta a/a$, %	R_{wp}, %	χ^2
		x	y	z				
$Dy_3Fe_5O_{12}$	12.409 (1)	0.974 (2)	0.062 (1)	0.151 (2)	39.1 (2)	23.9	11.9	1.29
$Ho_3Fe_5O_{12}$	12.366 (1)	0.963 (1)	0.063 (1)	0.157 (1)	42.9	19.8	12.3	1.33

provided. The TEM micrographs in Fig. 2 show dispersed parts of the samples, indicating that the particles are approximately spherical and adhere to one and another. By examining the particle sizes from various TEM images, the particle sizes of DyIGNPs are distributed in range of 20–50 nm with the most probable value of $D_{TEM} \sim 35$ nm and for HoIGNPs, the particle size range is 15–55 nm and D_{TEM} is ~38 nm (see the histograms on the right in Fig. 2). It is seen that the crystallite-size values D_{XRD} of the samples fall within the particle size ranges determined via TEM. EDX results in various investigated sample zones show that the atomic ratios $[R]/([R] + [Fe])$ of the samples are in agreement with those of the stoichiometric compositions within bounds of experimental error of this technique.

3.2. Magnetic characterization

The magnetization loops $M(H)$ of the samples in temperature range from 5 K to above the Curie temperature were measured. For demonstration, the hysteresis loops of the DyIGNP and HoIGNP samples at several temperatures are presented in Fig. 3. The curves show a linear behavior in high fields based on that the differential susceptibility value was determined. The spontaneous magnetization M_s was deduced by extrapolating the linear part of the curves to zero field. The coercivity H_c was also determined from the data. It is noted that at all investigated temperatures the full loop state was achieved in the samples under the experimental conditions.

3.2.1. Spontaneous magnetization M_s

The M_s versus T curves were shown in Fig. 4 from that the compensation temperature ($T_{comp} \sim 215$ K for DyIGNP and ~137 K for HoIGNP) and Curie temperature ($T_C \sim 550$ K for DyIGNP and ~560 K for HoIGNP) are found. The data of T_{comp} and T_C for bulk materials were reported by different sources as reviewed by Gilleo [7]. There is a discrepancy in these values, namely, T_{comp} was found in range 215–226 K for DyIG and 130–144 K for HoIG, T_C was reported to be 552 K or 563 K for DyIG and 558 K or 567 K for HoIG, which was attributed to inhomogeneity of the investigated samples [7 and references there in]. Pauthenet provided the spontaneous
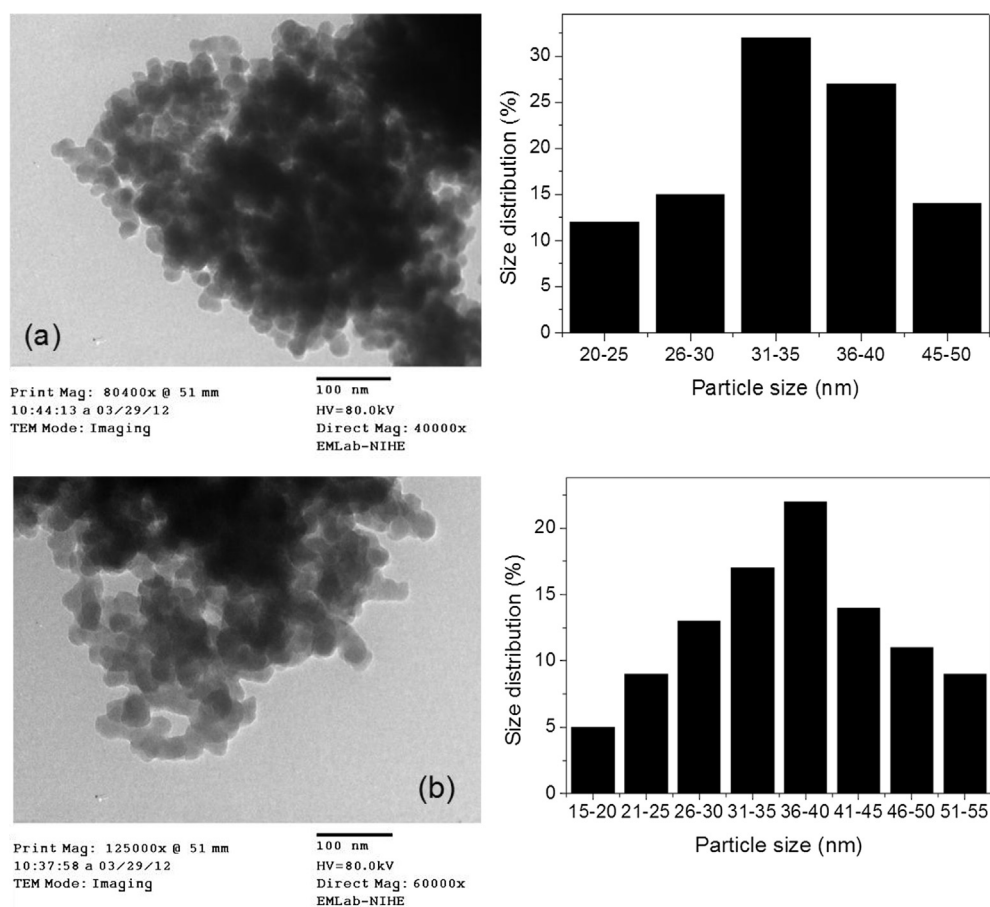

Print Mag: 80400x @ 51 mm
10:44:13 a 03/29/12
TEM Mode: Imaging

100 nm
HV=80.0kV
Direct Mag: 40000x
EMLab-NIHE

Print Mag: 125000x @ 51 mm
10:37:58 a 03/29/12
TEM Mode: Imaging

100 nm
HV=80.0kV
Direct Mag: 60000x
EMLab-NIHE

Fig. 2. TEM micrographs and histograms of size distribution of DyIGNPs (a) and of HoIGNPs (b).
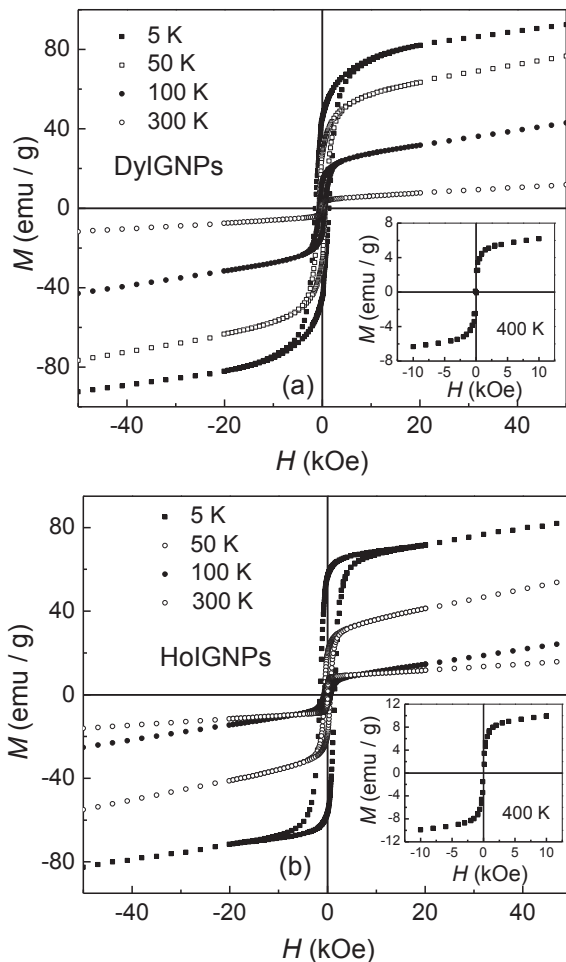
Fig. 3. Magnetization loops at $T = 5, 50, 100, 200, 300$ K of DyIGNPs (a) and of HoIGNPs (b). The insets show the loops at $T = 400$ K measured in maximum field of 10 kOe.
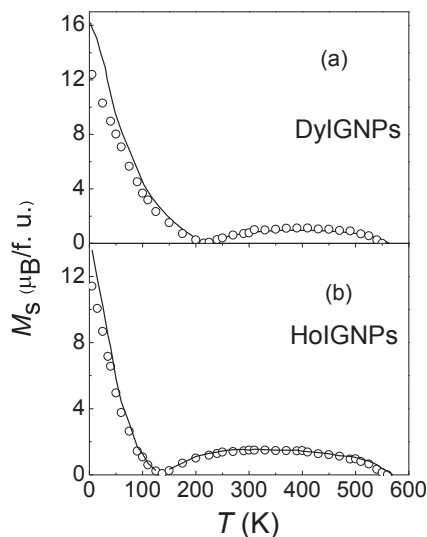

Fig. 4. Temperature dependence of the spontaneous magnetization M_s of DydIGNPs (a) and of HoIGNPs (b). The solid lines are the experimental data for bulk materials provided by Pauthenet [22] (see text).

magnetization of RIG samples in a wide temperature range from 2 K to above Curie temperature [22]. For comparison, the magnetization data measured for Dy and Ho compounds are also plotted in

the same graphs. It is seen that the T_{comp} values of the NP samples are in very good agreement with those of the bulks while their T_C values are several kelvins lower compared to the bulk values. The small difference between Curie temperatures of the NPs and of the bulks can be due to some causes such as the difference in homogeneity of the samples or the finite-size effect related to the nanoscale. For both samples, in temperature range $T < T_{comp}$ significantly lowering in the spontaneous magnetization M_s is observed while at $T > T_{comp}$, the M_s values of HoIGNPs recover to the bulk values and for DyIGNPs even slightly higher values were found. A similar but more pronounced effect was reported for GdIGNPs prepared by the same method [14].

At temperatures well below the compensation point, M_s of the NP samples is approximately 20% and 15% smaller compared to the bulk value for DyIG and HoIG, respectively. In order to explain this phenomenon we apply the core−shell model for these particles in which the core volume retains bulk behavior while the outer shell has deviated properties. The similarity in T_{comp} and T_C of the nanosized samples and bulks is due to the core and the lower magnetization compared to the bulk is attributed to the surface shell of the particles. In the surface region of the particles the variation in coordination of cations, broken exchange bonds or other types of defects occur which cause misalignment of the magnetic moments [23,24]. The size distribution of the particles also affects the magnetic properties because the contribution of the particles' surface to the magnetization of the samples becomes more significant as the particle size decreases. Assuming the magnetic moments in the outer shell are completely disordered and canceled out, the relation between the spontaneous magnetization of the nanoparticle sample (M_s^{exp}) and that of the bulk counterpart (M_s^{bulk}) can be described as

$$M_s^{exp} = M_s^{bulk}[(D/2 - t)/D/2]^3 \qquad (2)$$

for a spherical particle where D is the particle diameter and t the surface layer thickness. In order to estimate the surface layer thickness for the particles with diameter of D_{TEM}, the M_s^{exp} values are taken as M_s of DyIGNPs and HoIGNPs at 5 K, the M_s^{bulk} values of the bulks are taken from the M_s data at 5 K provided by Pauthenet [22]. The obtained values of t for DyIGNPs and HoIGNPs are respectively 1.4 nm and 1.1 nm which are within order of their lattice constants and hence are reasonable.

In rare-earth iron garnets, R-R and R-Fe magnetic interactions are very much weaker than Fe-Fe interactions [7,25,26] hence the rare-earth moments are expected to be more disordered than the iron spin system in the outer shell. As a result, the misalignment of the rare-earth moments at the surface is the main reason for the decrease in M_s at low temperatures because at these temperatures the rare-earth sublattice is the stronger magnetic sublattice. With increasing temperature above T_{comp}, the resultant Fe sublattice in the core volume becomes dominant whilst the rare-earth moments are largely decoupled from magnetic surroundings due to thermal perturbation as discussed in previous studies on bulk materials [19,25]. In surface region, due to the decoupling of rare-earth moments, the Fe spins can orient more easily to the direction of the magnetization of the core via Fe-Fe interactions which leads to an enhancement of the total magnetization. This mechanism can explain the recovery of M_s of the nanoparticles as comparing to the bulk values at high temperatures.

3.2.2. High-field susceptibility χ_{HF}

In Fig. 5, we show the temperature dependence of the high-field susceptibility χ_{HF} of the nanoparticle samples and of the bulks which were also reported by Pauthenet in [22]. At very low temperatures near 0 K the R ions in the bulk samples are almost
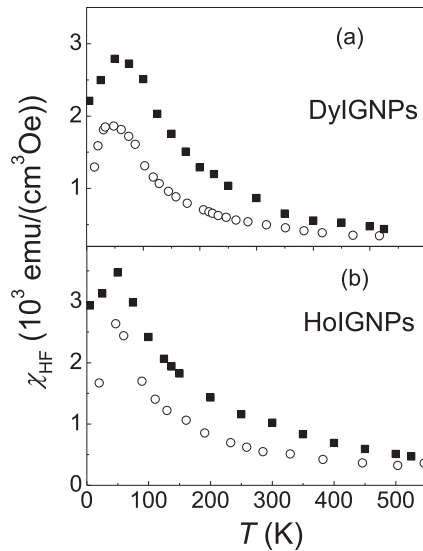
Fig. 5. Temperature dependence of the differential susceptibility χ_{HF} in high fields of DyIGNPs (a) and of HoIGNPs (b). The open circles are the experimental data for bulk materials provided by Pauthenet [22] (see text).

magnetically saturated due to the strong exchange field exerted by the Fe sublattices and hence χ_{HF} approaches zero. With increasing temperature, due to thermal excitation the R moments are partially demagnetized and there appears a differential susceptibility in presence of applied field, a process known as paraprocess. The χ_{HF} values reach a maximum below about 50 K and above that temperature the exchange forces acting on the R ions are overcome by the thermal energy, hence they are virtually free to orient in an applied magnetic field. The observed susceptibilities vary with temperature approximately as $1/T$ [22]. The temperature dependent behavior of the high-field susceptibility of the nanoparticle samples is similar to that of the bulks; however, their values are significantly higher in the whole investigated temperature range. This effect is attributed to the rotation of canted moments in the surface layer toward the applied field. Our previous study on GdIGNPs revealed that the contribution to the high-field susceptibility from the Gd spins at the surface is very huge which is manifested by a steep increase in χ_{HF} at low temperatures [14]. The variation of χ_{HF} versus T of this sample is therefore in opposite tendency compared to the bulk behavior. Much smaller contributions to χ_{HF} from the surface of the DyIGNPs and HoIGNPs observed in this work can be explained by non-S-state origin of R ions. The surface rare-earth moments are pinned by both exchange field and magnetocrystalline anisotropy field produced by the local electric field acting on their orbital moments, leading to small differential susceptibility at the surface with applying external field.

3.2.3. Magnetic coercivity H_c

Fig. 6 shows the results of measurement of the temperature dependence of H_c for the nanoparticle samples. For DyIGNP sample, a single peak in H_c is observed with the maximum value of 1.9 kOe located at T_{comp} (~225 K) while for HoIGNP sample, double peak is observed with two maxima H_c (125 K) = 1.35 kOe and H_c (150 K) = 1.15 kOe and a minimum at compensation point $H_c(T_{comp}\sim137$ K) = 250 Oe. Previous studies showed that these properties are inherent in RIG samples which exhibit T_{comp} [10,27–29]. Phenomenologically, the appearance of the double peak in H_c is consistent with the reduction of M_s to zero and so does H_c approach zero as temperature trespasses the compensation point. In reality, however, there always exist some lattice defects in
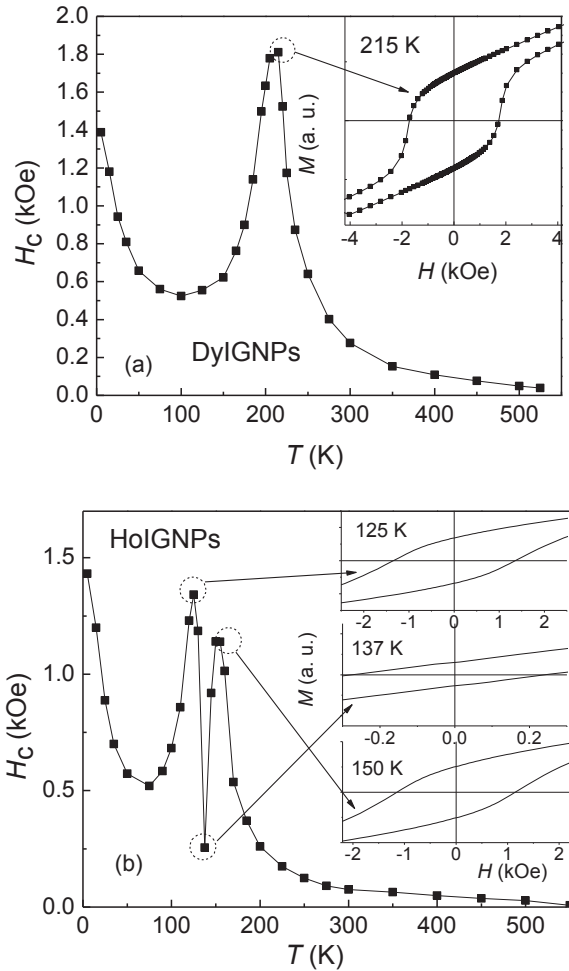

Fig. 6. Temperature dependence of the coercivity H_c of DyIGNPs (a) and of HoIGNPs (b). The insets are magnified parts of the hysteresis curves showing the highest and lowest values in the peak region around T_{comp}.

the samples leading to incomplete cancellation of sublattice magnetizations and hence non-zero H_c at T_{comp} is observed. It was also pointed out that in inhomogenous samples, single peak in H_c appears and the peak is broadened with increasing the degree of the inhomogeneity. Goranskiĭ and Zvezdin developed a theory based on the Stoner−Wolhfarth model in order to explain the formation of double peak in coercivity in such kind of materials [30]. In the theory it is assumed that near T_{comp} the spontaneous magnetization of the material is very small and hence its magnetostatic energy is negligible and the sample becomes a single domain. The magnetization process in this temperature region involves exclusively the rotation of magnetization vector. The difference between this theory and the Stoner−Wolhfarth model lies in the fact that the magnitude of the magnetization of the materials such as RIGs increases with increasing the applied field due to the paraprocess of the rare-earth sublattice. This process influences the shape of the hysteresis loops and is responsible for the formation of double peak in H_c near T_{comp} [10,30]. An expression for maximum coercivity was derived from the theory as follows [10]:

$$H_c(\max) = (aK/\chi)^{1/2} \qquad (3)$$

where K is anisotropy constant, χ susceptibility of the rare-earth sublattice, a the coefficient depending on the relative orientation of the applied field and the crystal axes. For the nanoparticle

samples, in the region around T_{comp}, K and χ are in order of 10^4 erg/cm^3 [31] and 10^{-3} emu/(cm^{3}Oe), respectively, therefore H_c is in order of 10^3 Oe according to Eq. (3), being in the same order of magnitude with the observed values (Fig. 6). Magnetic studies on RIG bulk samples reported much lower H_c(max) values, e.g. ~50 Oe for R = Dy, Ho in [24,25] or 600 Oe for R = Dy in [10]. The large difference in the experimental values of coercivity observed for bulk and nanosized forms suggests that the assumption of the single—domain state near T_{comp} in bulks may be an idealized concept. In [11], via the investigation of coercivity as a function of particle size Sánchez et al. showed that below a critical diameter $D_S \approx$ 190 nm, YIG particles become single domains. This result justifies that the particles in our samples are in single-domain state. On the other hand, in the bulk samples multi-domain structures are favorable. This can explain the larger coercivity of the nanosized samples compared to the bulks because the magnetization process in single-domain materials involves the rotation of magnetization whilst in multi-domain materials it takes place via movement of domain walls. Another reason for the low H_c values observed in [27] and [28] for bulk samples may also be due to the fact that the maximum applied fields used in these studies were not large enough to create the full loop states.

At low temperature range far apart from the peak region, an increasing tendency of H_c with deceasing temperature is observed which is mostly originated from the increase of magnetocrystalline anisotropy as a result of the ordering of the rare-earth sublattice. For both samples, at 5 K the coercivity reaches about 1.4 kOe. The H_c values of the investigated samples also depend on other factors such as the statistical distribution of the crystallographic directions of the particles in the assembly, the number of metastable orientations of particle moments defined by the competition between the core and the surface anisotropy contributions and the interactions between them.

4. Conclusion

DyIG and HoIG nanoparticles were successfully prepared by citrate sol-gel technique with subsequent calcination at 800 °C for 2 h. Crystal structure and magnetic analyses have shown that the samples are in single phase with high degree of crystallinity and have fairly good chemical homogeneity. The particles can be treated in the core-shell morphology in which the core inherits the bulk properties and the shell has deviated properties. Because the core part has the main contribution to the magnetization of the systems, the values of Curie and compensation temperature of the nanosized samples are similar to those of the bulks. On the other hand, compared to the bulks higher magnetic susceptibility in high fields is observed for the nanoparticles due to the disorder nature of the surface spins. Because the particles are in single-domain state, the nanosized samples show a very large coercivity in comparison with the bulks. In particular, a double peak in H_c around compensation point was observed for HoIGNPs which agrees well with the theoretical model developed for coercivity of RIG materials associated with magnetization compensation phenomenon. This also indicates that the HoIGNP sample has better homogeneity than the DyIGNP one which shows a single peak in H_c near T_{comp}. This study together with our recent studies [13,14] have contributed to the systematic view on the magnetic properties of RIG nanoparticles with size distribution in approximate range 20—55 nm. The studies also show that sol—gel is an efficient route for fabricating nanosized garnets. Further studies on valence states of the magnetic cations as well as surface spin states are particularly helpful in understanding the origins of magnetic phenomena of this type of materials at nanoscale.

References

[1] F. Tcheou, E.F. Bertaut, H. Fuess, II − Neutron diffraction study of some rare earth iron garnets RIG (R = Dy, Er, Yb, Tm) at low temperaures, Solid State Commun. 8 (1970) 1751−1758.

[2] G. Winkler, Magnetic Garnets, Friedr. Vieweg and Sohn, Braunschweig/Wiesbaden, 1981.

[3] S. Taketomi, C.M. Sorensen, K.J. Kabunde, Prepareration of yttrium iron garnet nanocrystals dispersed in nanosize pore glass, J. Magn. Magn. Mater. 222 (2000) 54−64.

[4] R. Fujikawa, A.V. Baryshev, J. Kim, H. Uchida, M. Inoue, Contribution of the surface plasmon resonance to optical and magneto-optical properties of a Bi:YIG-Au nanostructure, J. Appl. Phys. 103 (2008), 07D301-303.

[5] T.V. Murzina, A.A. Nikulin, O.A. Aktsipetrov, J.W. Ostrander, A.A. Mamedov, N.A. Kotov, M.A.C. Devillers, J. Roark, Nonlinear magneto-optical Kerr effect in hyper-Rayleigh scattering from layer by layer assembled films of yttrium iron garnet nanoparticles, Appl. Phys. Lett. 79 (2001) 1309.

[6] A.M. Tishin, Y.I. Spichkin, The Magnetocaloric Effect and Its Applications, IOP Publishing Ltd, 2003.

[7] M.A. Gilleo, in: E.P. Wohlfarth (Ed.), Ferromagnetic Materials: A Handbook of the Properties of Magnetically Ordered Substances vol. 2, North-Holland, Amsterdam, 1980 (Chapter 1).

[8] W. Wang, R. Chen, X. Qui, Analysis on three-sublattice model of magnetic properties in rare-earth iron garnets under high magnetic fields, J. Alloy Compd. 512 (2012) 128.

[9] M. Lahoubi, W. Younsi, M.-L. Soltani, B. Ouaddiaf, Anisotropic magnetic properties of dysprosium iron garnet (DyIG), J. Phys. Conf. Ser. 200 (2010) 082018.

[10] M. Uemura, T. Yamagishi, S. Ebisu, S. Chikazawa, S. Nagata, A double peak of the coercive force near the compensation temperature in the rare earth iron garnets, Philos. Mag. 88 (2008) 209−228.

[11] R.D. Sánchez, J. Rivas, P. Vaqueiro, M.A. Lopez-Quintela, D. Caeiro, Particle size effects on magnetic properties of yttrium iron garnets prepared by a sol−gel method, J. Magn. Magn. Mater. 247 (2002) 92−98.

[12] M. Rajendran, S. Deka, P.A. Joy, A.K. Bhattacharya, Size-dependent magnetic properties of nanocrystalline yttrium iron garnet powders, J. Magn. Magn. Mater. 301 (2006) 212−219.

[13] Dao Thi Thuy Nguyet, Nguyen Phuc Duong, Takuya Satoh, Luong Ngoc Anh, Than Duc Hien, Temperature-dependent magnetic properties of yttrium iron garnet nanoparticles prepared by citrate sol−gel, J. Alloy Compd. 541 (2012) 18−22.

[14] Dao Thi Thuy Nguyet, Nguyen Phuc Duong, Takuya Satoh, Luong Ngoc Anh, Than Duc Hien, Magnetization and coercivity of nanocrystalline gadolinium iron garnet, J. Magn. Magn. Mater 332 (2013) 180−185.

[15] R. Tholkappiyan, K. Vishista, Tuning the composition and magnetostructure of dysprosium iron garnets by Co-substitution: an XRD, FT−IR, XPS and VSM study, Appl. Surf. Sci. 351 (2015) 1016.

[16] M. Guillot, C.N. Chinnasamy, J.M. Greneche, V.G. Harris, Tuning the cation distribution and magnetic properties of single phase nanocrystalline Dy3Fe5O12 garnet, J. Appl. Phys. 111 (2012), 07A517.

[17] C.N. Chinnasamy, J.M. Greneche, M. Guillot, B. Latha, T. Sakai, C. Vittoria, V.G. Harris, Structural and size dependent magnetic properties of single phase nanostructured gadolinium-iron-garnet under high magnetic field of 32 tesla, J. Appl. Phys. 107 (2010), 09A512.

[18] A.E. Berkowitz, W.J. Schuele, P.J. Flanders, Influence of crystallite size on the magnetic properties of acicular γ-Fe2O3 particles, J. Appl. Phys. 39 (1968) 1261.

[19] A.H. Morrish, K. Haneda, Non-collinearity as a cystallite-size effect of γ-Fe2O3 small particles, J. Phys. Colloq. 41 (1980) C1−C171.

[20] J. Rodriguez-carvajal, Structural Analysis from Powder Diffraction Data the Rietveld Method, Ecole Thématique: Cristallograpie et Neutrons 418, 1997, p. 73.

[21] L.B. Mc Cusker, R.B. Von Dreele, D.E. Cox, D. Louër, P. Scardi, Rietveld refinement guidelines, J. Appl. Crystallogr. 32 (1999) 36−50.

[22] R. Pauthenet, Les propriétés magnéues des ferrites d'yttrium et de terres rares de formule 5Fe2O3.3M2O3, Ann. Phys. 3 (1958) 424−462.

[23] A. Labarta, X. Batle, O. Iglesias, in: D. Fiorani (Ed.), Surface Effects in Magnetic Nanoparticles, Springer, 2005 (Chapter 4).

[24] R.H. Kodama, A.E. Berkowitz, E.J. McNiff, S. Foner, Surface spin disorder in NiFe2O4 nanoparticles, Phys. Rev. Lett. 77 (1996) 394−397.

[25] K.P. Belov, S.A. Nikitin, Zur theorie der tieftemperatur-anomalien in den ferrit-granaten seltener erden, Phys. Status Solidii 12 (1965) 453−464.

[26] G.F. Dionne, Molecular field and exchange constants of Gd^{3+} substituted ferrimagnetic garnets, J. Appl. Phys. 42 (1971) 2142−2143.

[27] K.P. Belov, R.Z. Levitin, S.A. Nikitin, A.V. Ped'ko, Magnetic and magnetoelastic properties of dysprosium and gadolinium, Sov. Phys. JETP 13 (1961) 1096–1101.

[28] J.P. Hanton, Intrinsic coercive force of rare earth iron garnets near the compensation temperature, IEEE Trans. Magn. 3 (1967) 505–509.

[29] C.D. Mee, The magnetization mechanism in single crystal garnet slabs near the compensation temperature, IBM J. Res. Dev. 11 (1967) 468–476.

[30] B.P. Goranskiĭ, A.K. Zvezdin, Temperature dependence of the coercive force of ferrimagnets near the compensation temperature, Sov. Phys. JETP 30 (1970) 299–301.

[31] R.F. Pearson, Magnetocrystalline anisotropy of rare-earth iron garnets, J. Appl. Phys. 33 (1962) 1236–1242.